JOURNAL OF SOLID STATE CHEMISTRY 100, 341–355 (1992)

Single-Crystal Structure Determination of γ-Ag_8SiTe_6 and Powder X-ray Study of Low-Temperature α and β Phases

F. BOUCHER, M. EVAIN,* AND R. BREC

I.M.N., Laboratoire de Chimie des Solides, 2 rue de la Houssinière, 44072 Nantes Cedex 03, France

Received January 16, 1992; in revised form March 26, 1992; accepted March 30, 1992

γ-Ag_8SiTe_6 crystallizes in the cubic symmetry with $a = 1152.25(7)$ pm, space group $F\bar{4}3m$, $Z = 4$. The structure was solved from 316 independent reflections, and anisotropic least-squares refinements gave $R = 0.029$ with 32 variables. The structure consists of a framework of $SiTe_4$ tetrahedra and Te atoms; the Ag atoms are disordered among "clusters" built upon $AgTe_4$ tetrahedra and interstitial sites. Powder X-ray studies of the low-temperature α- and β-Ag_8SiTe_6 phases indicate a cubic system with a symmetry lowering, from face-centered to primitive, and a parameter change from a to $\approx 2a$.

Introduction

Numerous papers have been published on silver-containing ionic conductors. In these compounds, the Ag^+ ions are free to move within a three-dimensional framework, thus yielding an ionic conductivity. For instance, in AgI (*1*) the iodine network induces large cavities the silver ions can transit through. Ag_2Te (*2*) presents the same characteristic except that, beside the ionic conduction, it has an electronic conductivity (*3*). In both compounds, e.g., AgI and Ag_2Te, the ionic conductivity is noticeable only for the high-temperature allotropic phases which are stable above 146 and 150°C, respectively. In Ag_4RbI_5 the alkali metal decreases the temperature onset of the higher conducting phase (−155°C) with still a high ionic conductivity. Similarly, the addition of silicon or germanium in the Ag–Te system generates new phases (Ag_8MTe_6) with ion conducting, high-temperature allotropic forms stable around room temperature.

Although the Ag_8MTe_6 phases (M = Si or Ge), and more generally the Ag_8MX_6 phases (M = Si, Ge, or Sn and X = S, Se, or Te, not all the combinations having being observed), have been known for some time (*4–8*), their structures or more precisely the structures of their high-temperature allotropic forms are still unknown or, if known, often inaccurate. For instance, if we restrict ourselves to the tellurium family, we notice that the structure of γ-Ag_8SiTe_6 is unknown and that the structure of γ-Ag_8GeTe_6 was first described as cubic (*9*), was then shown to be rhombohedral (*10*), and later again described as cubic (*11*). For the latter phase, if there is no doubt about the location of the tellurium and germanium atoms, there is still suspicion about the real position of the silver ions, even in the rhombohedral description of the structure in which one calculates un-

* To whom correspondence should be addressed.

0022-4596/92 $5.00

realistic distances such as $d_{Ge-Ag13} = 256$ pm (same order of length as the germanium to tellurium distances!) and $d_{Ag5-Te2} = 216$ pm (quite a short distance even in a linear arrangement). Being particularly interested in d^{10} cation behavior (*12*) we decided to tackle the problem of silver situation in the Ag_8MX_6 phases and in particular in Ag_8SiTe_6. In this paper, we report the room-temperature, single-crystal structure determination of γ-Ag_8SiTe_6 and a powder X-ray study of the low-temperature α and β phases.

Experimental

Synthesis. γ-Ag_8SiTe_6 was synthesized by direct combination of the elements in an evacuated quartz tube. Large crystals were easily obtained for a nonstoichiometric 5 : 1 : 4 ratio, the samples being heated at 800°C for 7 days and subsequently cooled to 500°C over a 6-day period and then to room temperature within a day. Since a single crystal small enough for X-ray studies could not be found, a block of proper size ($\approx$0.08 $\times$ 0.08 $\times$ 0.04 mm^3) was fashioned from a large one by cutting it in arbitrary directions. For the powder work, several crystals were cleaned and isolated in hexane and then ground and passed through a 50-μm mesh sieve.

An analysis by means of a microprobe (SEM) led to Ag, 48.5%; Si, 9.05%; and Te, 42.45%. That semiquantitative analysis departs substantially from calculated values (Ag, 53.3; Si, 6.7; and Te, 40.0) and should be cautiously considered.

Powder pattern analysis. Powder patterns were obtained, at room temperature, on a Siemens D5000 diffractometer with a strictly monochromatic Cu$K_{\alpha 1}$ radiation. The specimen displacement was compensated for by using a standard material (Cr_2O_3) as an internal reference sample. The data were collected in steps of 0.02° (2θ) with 50-sec counting periods over a 10°–140° range (2θ). The powder patterns were processed with the PROLIX program (*13*) including several options such as background stripping, peak search, and profile-fitting.

TABLE I

γ-Ag_8SiTe_6 INDEXED POWDER PATTERN

d_{obs}(pm)	d_{cal}(pm)	$h\ k\ l$	I_{rel}
665.8	665.2	1 1 1	8
347.47	347.42	3 1 1	41
332.68	332.62	2 2 2	93
264.38	264.34	3 3 1	11
257.63	257.65	4 2 0	3
235.22	235.20	4 2 2	24
221.76	221.75	3 3 3	100
203.69	203.69	4 4 0	48
194.757	194.765	5 3 1	12
192.027	192.041	4 4 2	3
182.197	182.186	6 2 0	3
175.719	175.716	5 3 3	8
173.693	173.708	6 2 2	9
166.323	166.313	4 4 4	2
161.333	161.347	5 5 1	4
150.012	150.010	5 5 3	8
135.777	135.794	8 2 2	4
133.041	133.050	5 5 5	7
132.166	132.172	6 6 2	8
128.841	128.825	8 4 0	3
126.470	126.476	7 5 3	3
120.802	120.788	9 3 1	5
117.597	117.601	8 4 4	7
110.885	110.875	6 6 6	3
101.838	101.845	8 8 0	3
100.673	100.672	9 5 5	3

The cubic parameter $a = 1152.25(7)$ pm was least-squares refined from 26 reflections with an average discrepancy in 2θ of 0.0048° (see Table I). This cell constant agrees well with that of Gorochov (*8*) $a = 1151.5$ pm (F centering). Only one very small line (2θ = 26.4°) could not be indexed. It corresponds to the strongest line of Si_2Te_3 that comes in as impurity because of the nonstoichiometry of the starting mixture (platelets of that phase have been noticed in raw samples).

Single-crystal study. Conventional film studies (rotation and Weissenberg) on the

TABLE II

ANALYTICAL AND CRYSTALLOGRAPHIC DATA: PARAMETERS OF THE X-RAY DATA COLLECTION AND REFINEMENT

Physical, crystallographic, and analytical data	
Formula:	Ag_8SiTe_6 Space group: $F\bar{4}3m$ (no. 216)
Room temperature crystallographic constants:	
	$a = 1152.25(7)$ pm $Z = 4$
Molecular weight:	1656.6 g/mol Density (calc.): 7.192
Absorption factor: $\mu(MoK\alpha) = 212.4$ cm^{-1}	
Crystal size $< 0.08 \times 0.08 \times 0.04$ mm^3	
Data collection	
Temperature:	293 K
Radiation: MoK_α	Monochromator: oriented graphite (002)
Scan mode: $\omega/2\theta$	Scan angle: $1.5 + 0.35 \tan(\theta)$
Recording range: 2–35°	
Standard reflections: 3 3 3, 2 6 6, 8 8 0 (every 3600 sec)	
Refinement conditions	
Reliability factors	$R = \Sigma(\|\|F_o\| - \|F_c\|\|)/\Sigma\|F_o\|$
	$R_w = (\Sigma w(\|F_o\| - \|F_c\|)^2/\Sigma wF_o^2)^{\frac{1}{2}}$
Goodness-of-fit (error in an observation of unit weight):	
	$S = [\Sigma w(\|F_o\| - \|F_c\|)^2/\text{degrees of freedom}]^{\frac{1}{2}}$
Weighting scheme: $1/\sigma(F)^2$	
Refinement results	
$R = 2.9\%$	$Rw = 3.5\%$ $S = 1.06$
Extinction coefficient: $E_c = 2.00(4) \times 10^{-6}$	
Difference Fourier maximum peak intensity: $2.2(3) \times 10^{-6}$ e$^-$/pm^3	

chosen crystal confirmed the faced-centered cubic symmetry. The data collection was performed on a CAD4 Enraf–Nonius diffractometer (monochromatized MoK_α radiation) in a standard way (see Table II). Omitting systematically absent reflections, 3494 *hkl* were measured in the *-h/h, -k/k,* and *0/l* reciprocal space. Because of the undefined shape of the crystal, a Psi measurement on nine reflections (χ close to 90°) was carried out for a subsequent empirical absorption correction. After the usual corrections (decay, absorption, and Lorentz-polarization) a set of 2620 reflections verified the $I > 3\sigma(I)$ condition. Conforming to the noncentrosymmetric character of that set, three space groups, $F432$, $F\bar{4}3m$, and $F23$, could be assumed. We retained $F\bar{4}3m$ that was precedently chosen in the Ag_8GeTe_6 structural determination (*9, 11*). Thus equivalent reflections were averaged according to the Laue symmetry $\bar{4}3m$ (agreement factor for accepted reflections: 0.030 on F_{obs} and 0.044 on I) yielding 316 independent *hkl* with $I > 3\sigma(I)$ for structural refinements.

Structure Refinement

All structural refinements were carried out with the MOLEN chain program (*14*). The Patterson map analysis revealed tellurium positions identical to those obtained by

Geller in Ag_8GeTe_6 (*11*) (i.e., 16e, 4*c*, and 4*a*). A first refinement series with those tellurium sites and the silicon tetrahedral position (4*d*) led to the reliability factor R = 25.7%. A Fourier difference map exhibited a silver tetrahedral site (Ag1 in 48*h*). With this new position and a refinement of its occupancy factor the R value dropped to 15%. At this stage of the refinement process, Fourier and Fourier-difference maps suggested two new residues of minor but significant intensity. The introduction of those new silver sites, Ag2 and Ag3 with refinement occupancy ratios, and anisotropic temperature factors considerably improved the reliability factor (5%). Finally, taking into account the secondary extinction coefficient and with a $1/\sigma^2$ weighting scheme, the final confidence factors converged to R_W = 3.5%, R = 2.9%, and S = 1.06. Then, an ultimate Fourier difference map showed only minor residual density (max = 2.2 × 10^{-6} e^-/pm^3) around tellurium positions. Fractional coordinates, occupancy factors, and thermal parameters of the seven independent atoms of the cell are gathered in Tables IIIa and IV, respectively.

Structural Results

The unit cell is made of four basic Ag_8SiTe_6 units (Z = 4), i.e., 32 silver atoms, 4 silicon atoms, and 24 tellurium atoms. As already noted by Geller (*11*), the Te arrangement is similar to that of Mg and Cu in the $MgCu_2$ Friauf–Laves phase. This phase crystallizes in the cubic system, space group $Fd3m$, with the Mg atoms in the 8*a* positions: 0, 0, 0; $\frac{1}{4}$, $\frac{1}{4}$, $\frac{1}{4}$, and the Cu atoms in 16*d*: $\frac{5}{8}$, $\frac{5}{8}$, $\frac{5}{8}$; $\frac{5}{8}$, $\frac{7}{8}$, $\frac{7}{8}$; $\frac{7}{8}$, $\frac{5}{8}$, $\frac{7}{8}$; $\frac{7}{8}$, $\frac{7}{8}$, $\frac{5}{8}$ (plus cell-centering). Indeed, we observe in Ag_8SiTe_6 one tellurium (Te3) in 4*a*: 0, 0, 0; another one (Te2) in 4*c*: $\frac{1}{4}$, $\frac{1}{4}$, $\frac{1}{4}$; and the last one (Te1) in 16*e*: x, x, x; x, $-x$, $-x$; $-x$, x, $-x$; $-x$, $-x$, x (x = 0.62532(7) ≈ $\frac{5}{8}$) (see Table IIIa). Those last Te1 sites pattern regular tetrahedral sites in which lie silicon atoms (4*d* positions: $\frac{3}{4}$, $\frac{3}{4}$, $\frac{3}{4}$). The remaining atoms (the 32 silver atoms) partially occupy three sites, two of them presenting very high Atomic Displacement Parameters (ADP) (see below for the reason of using "ADP" instead of "thermal motion parameters"). The minor site, Ag1, fills up 16.8(2)% of a 48*h* position and exhibits a high but reasonable B_{eq} value (3.55(5) × 10^4 pm^2). The two other sites, Ag2 and Ag3, take up 25.6(2) and 12.2(1)% of a 48*h* and a 96*i* position, respectively, and show huge B_{eq} (13.16(5) × 10^4 and 14.6(2) × 10^4 pm^2, respectively). The total amount of silver (32.0(3)) perfectly matches the stoichiometry of the title formula.

Description

To better grasp the overall structural arrangement, we first describe the "$SiTe_6$" ordering. As already mentioned, the Te3 sites are located at the apexes of the primitive lattice cell, that is, at the corners and in the middle of the faces of the F centered cell, thus framing 8 tetrahedral sites. Each tetrahedral site is occupied either by an $SiTe_4$ group or by a tellurium atom (Te2 type), and this in an alternate way (see Fig. 1).

An attentive inspection of the equivalent ADP (B_{eq}) of silicon and tellurium atoms (Table IV) evidences that:

—the $SiTe_4$ group is well defined, e.g., the B_{eq} of silicon (0.77 × 10^4 pm^2) and of tellurium (1.722 × 10^4 pm^2) are comparable to what is usually observed, as in $Cr_2Si_2Te_6$ (*15*) (1.10 × 10^4 pm^2 for Si and 1.05 × 10^4 pm^2 for Te).

—the Te2 and Te3 ions exhibit relatively large ADP values (B_{eq} = 4.83 × 10^4 and 5.56 × 10^4 pm^2, respectively). As Rysanek (*9*) and Geller (*11*) already discussed, contrary to Te1, Te2, and Te3 anions are only coordinated to silver cations. Consequently, the

TABLE IIIa

ATOMIC REFINED POSITIONS (MEANS), ISOTROPIC EQUIVALENT ATOMIC DISPLACEMENT PARAMETERS (ADP), AND THEIR ESTIMATED STANDARD DEVIATIONS

Atom	x	y	z	B_{eq} $(\times 10^{-4})^a$	τ
Si	$\frac{3}{4}$	$\frac{3}{4}$	$\frac{3}{4}$	0.77(2)	
Te1	0.62532(7)	0.625	0.625	1.722(2)	
Te2	$\frac{1}{4}$	$\frac{1}{4}$	$\frac{1}{4}$	5.56(2)	
Te3	0	0	0	4.83(2)	
Ag1	0.4281(3)	0.428	0.2230(4)	3.55(5)	0.168(2)
Ag2	0.4622(4)	0.462	0.2281(3)	13.16(5)	0.256(2)
Ag3	0.3680(7)	0.4369(4)	0.2249(7)	14.6(2)	0.122(1)

[a] Isotropic equivalent ADP defined as B_{eq} (pm^2) $= \frac{4}{3}\Sigma_i\Sigma_j\beta_{ij}a_ia_j$.

apparent thermal motion of the Te2 and Te3 sites is directly related to the large distribution observed on the silver neighboring sites (this is the reason why we do prefer to use the "Atomic Displacement Parameter" qualifier rather than the usual "thermal parameter" notion, the ADP covers on the one hand traditional thermal vibrations and, on the other hand, distributions).

Thus, as Krebs previously suggested for Ag_8SiS_6 (*16*), it can be stated that the Ag_8SiTe_6 structure is built upon $(SiTe_4)^{4-}$ entities linked through silver and tellurium (Te2 and Te3) atoms. The phase can therefore be reformulated as $Ag_8(SiTe_4)Te_2$.

Within each $SiTe_4$ cluster, the Te1–Te1 distances (406.4(1) and 408.4(1) pm, see Table V) relate to that observed in close-packing arrangements (from 396.66(5) pm to 437.14(5) pm in $Mn_3Si_2Te_6$ (*17*); from 372.8(5) pm to 424.9(3) pm in $Cr_2Si_2Te_6$(*15*)). The Si–Te1 distance (248.84(6) pm) checks well with the Shannon previsions (*18*) (r^{4+}_{Si} = 42.5 pm; r^{2-}_{Te} = 207 pm).

TABLE IIIb

ESTIMATED SILVER LOCAL MAXIMA (MODES)

Atom	x	y	z
Ag1*	0.427	0.427	0.228
Ag2*	$\frac{1}{2}$	$\frac{1}{2}$	0.208
Ag3*	0.361	0.441	0.219

Let us carry on the description by looking at the various tetrahedral voids present in the structure, whether there are filled or not by silver atoms. The $SiTe_6$ framework manages a total of 132 tetrahedral sites that can be reduced to only five different types (as described by Rysanek *et al.* (*9*)). The stereoscopic view of the $SiTe_6$ skeleton (Fig. 1) allows to easily locate those sites. Since the occupation of such voids by the silver cations is mainly governed by the proximity of the silicon cations (because of the electrostatic repulsion), let us characterize the tetrahedron types, not only by a review of the apexes they originate from, but also by the distance from its center to the closest silicon atom (d_{C-Si}):

—build upon 2 Te1, 1 Te2, and 1 Te3 atoms, the 48 tetrahedra of type I share an edge with an $SiTe_4$ entity; a distance d_{C-Si} = 306 pm is calculated.

—the tetrahedra of type II (16 per cell) are the only ones that have a common face (3 × Te1) with an $SiTe_4$ group (the last corner

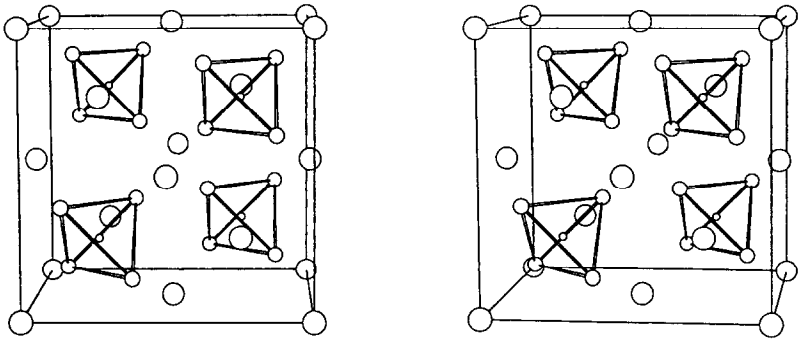

FIG. 1. Ortep stereoscopic view of the $SiTe_6$ framework of γ-Ag_8SiTe_6. Spheres of arbitrary size (large for Te2 and Te3, medium for Te1, and small for Si) are used to depict the tellurium and silicon atoms.

TABLE IV

ATOMIC DISPLACEMENT PARAMETERS (ADP): Us ($\times 10^{-4}$ pm^2)

Atom	U_{11}	U_{22}	U_{33}	U_{12}	U_{13}	U_{23}
Si	0.0098(9)	U_{11}	U_{11}	0	0	0
Te1	0.0218(1)	U_{11}	U_{11}	−0.0044(1)	U_{12}	U_{12}
Te2	0.0704(9)	U_{11}	U_{11}	0	0	0
Te3	0.0612(7)	U_{11}	U_{11}	0	0	0
Ag1	0.054(1)	U_{11}	0.027(2)	−0.008(2)	−0.007(1)	U_{13}
Ag2	0.212(1)	U_{11}	0.075(2)	0.177(2)	−0.106(1)	U_{13}
Ag3	0.259(6)	0.079(3)	0.217(6)	−0.102(3)	0.149(6)	−0.092(3)

Note. The expression of the general temperature factor is $\exp[-2\pi^2 (U_{11}h^2a^{*2} + U_{22}k^2b^{*2} + U_{33}l^2c^{*2} + 2U_{12}hka^*b^* + 2U_{13}hla^*c^* + 2U_{23}klb^*c^*)]$.

TABLE V

MAIN INTERATOMIC DISTANCES (pm) AND ANGLES (°) BASED UPON THE LOCAL MAXIMA OF THE pdf (MODES) IN γ-Ag_8SiTe_6

Si –Te1	248.84(6) (×4)		
Te1 –Te1	408.4(1) (×3)		
Te1 –Te1	406.4(1) (×3)		
Ag1*–Te1	291 (×2)	Te1–Ag1*–Te1	89.3
Ag1*–Te2	290	Te1–Ag1*–Te2	110.7 (×2)
Ag1*–Te3	288	Te1–Ag1*–Te3	111.3 (×2)
	$(Ag1^*–Te)_{avr}$: 290	Te2–Ag1*–Te3	119.4
Ag2*–Te1	281 (×2)	Te1–Ag2*–Te1	93.3
Ag2*–Te3	239	Te1–Ag2*–Te3	133.3 (×2)
	$(Ag2^*–Te)_{avr}$: 267		
Ag3*–Te1	279	Te1–Ag3*–Te2	126.5
Ag3*–Te2	256	Te1–Ag3*–Te3	109.2
Ag3*–Te3	307	Te2–Ag3*–Te3	124.3
	$(Ag3^*–Te)_{avr}$: 281		

being a tellurium Te3). They imply a very short center to silicon distance d_{C-Si} = 187 pm.

—for the third type (type III, 4 entities), each tetrahedron is made of four corners (Te1) of four different $SiTe_4$ groups (d_{C-Si} = 499 pm).

—the type IV tetrahedra are very similar to those of type I (2 × Te1, 1 × Te2, 1 × Te3, (d_{C-Si} = 420 pm)). There are 48 sites of that type. Type IV tetrahedra share two corners with two different $SiTe_4$ tetrahedra.

—finally, the tetrahedra of the last type (type V) have one face in common with those of type III (3 × Te1) and thus share three corners with $SiTe_4$ groups, the last corner being of a Te2 tellurium. We list 16 such tetrahedra and calculate d_{C-Si} = 471 pm.

Of the five types only two are of importance for the silver distribution: the type I and IV, that is, a total of 96 tetrahedra (a reason why the other three types could probably not be taken into account will be given at the end of this section). Ag1 occupies a site of type IV (16.8% of the full site occupation); the Ag2 refined position is located in the triangular face common to two type IV tetrahedral sites (25.6% of the full occupancy); the Ag3 refined position is in a site common to a tetrahedron of type I and to a tetrahedron of type IV (12.2% of the full occupancy). Therefore, the centers of type I tetrahedra are also vacant and only the type IV sites are partially filled.

From the ADP values (Tables IIIa and IV), we observe that, out of the three silver atoms, Ag1 is the only one which is well defined with a $B_{eq} = 3.55(5) \times 10^4$ pm^2. This high but reasonable equivalent isotropic factor is a common trend of d^{10} elements (*19*). For example, in $AgVP_2S_6$ (*20*) B_{eq} (octahedral Ag) = 3.10×10^4 pm^2, in $Ag_4P_2S_6$ (*21*) B_{eq} (tetrahedral Ag) = 3.6×10^4 pm^2, in average, and in $ZnPS_3$ (*22*) B_{eq} (octahedral Zn) = 1.9×10^4 pm^2. On the contrary, the ADP of the other two silver positions are remarkably high and very anisotropic, e.g., $B_{eq} = 14.6 \times 10^4$ pm^2 and $U_{11} = U_{22} \approx 3 \times U_{33}$ for Ag2 and $B_{eq} = 13.2 \times 10^4$ pm^2 and $U_{11} \approx U_{33} \approx 3 \times U_{22}$ for Ag_3. Those silver positions are not "true sites" but simply correspond to a non-vanishing probability density in the vicinity of the tetrahedral faces; that is, they are a mathematical expression either of a cationic diffusion path (dynamic disorder) or of multiple positions (static disorder) (*23*). Because of the overlap between the probability density function (*pdf*) of the various silver atoms, one should not consider the individual *pdf* but the joint probability density function (*jpdf*) (*24*) and should not discuss about the different structural environments from the refined positions but from the maxima of the *jpdf*. The *jpdf* of an atom type k at position $\mathbf{r}$ is given by

$$jpdf_k(\mathbf{r}) = \sum_i \omega_{ik}\, pdf_{ik}(\mathbf{r})$$

where ω_{ik} is the occupancy of position i by an atom of type k and the sum is taken over all positions that can be occupied by the atoms of type k.

Before considering the true maxima of the jpdf, let us first describe the global arrangement of silver atoms in the Ag_8SiTe_6 structure from the refined positions. In Fig. 2 we present the overall arrangement of the tetrahedra of type I and type IV. Each type IV tetrahedron (partially occupied by Ag1) shares a face with another type IV tetrahedron and two faces with two type I tetrahedra. The former face type is occupied by Ag2 and the latter by Ag3. This arrangement and the observed direction of the ADP values suggest a diffusion path of the silver ions from one type IV tetrahedral site to another type IV tetrahedral site

—either directly through their common face,

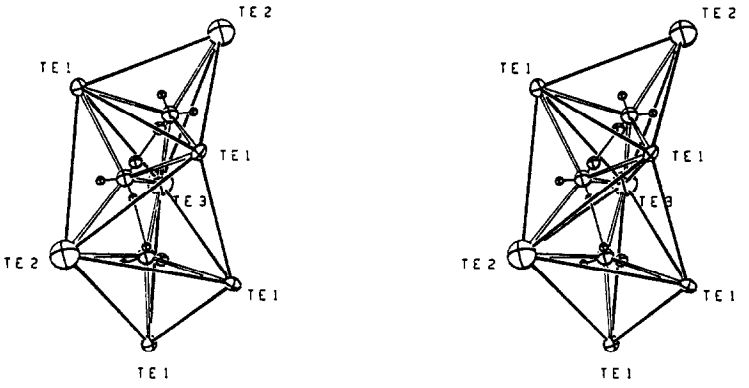

FIG. 2. Ortep stereoscopic view of refined silver positions in adjacent type IV tetrahedra. ADP ellipsoids are presented for tellurium atom only; spheres of arbitrary size (large for Ag1, medium for Ag2, and small for Ag3) are used to depict the silver atoms because of the density overlap.

$$Ag1 \leftrightarrow Ag2 \leftrightarrow Ag2 \leftrightarrow Ag1$$

—or indirectly through their common edge and through adjacent type I tetrahedra,

$$Ag1 \leftrightarrow Ag3 \leftrightarrow Ag3 \leftrightarrow Ag1$$

In Figs. 3a and 3b we present the jpdf along the direct and indirect jump, respectively. On both figures clearly appears the ionic diffusion path between the adjacent tetrahedra. In Fig. 3a we observe that the Ag2 refined position does not correspond to a density probability maximum (mean and mode definition (*25*): the mean is the refined atom position, the mode is given by the local maximum of the jpdf), the maximum being in the triangular face; let us label Ag2* that position. On Fig. 3b no real maximum shows up; a continuous path of density probability spread from one Ag1 position to the neighboring one. We label Ag3* the intersection of the locus of the maximum of density and the tetrahedron faces. We also rename Ag1 as Ag1* for convenience but the maximum of density near Ag1 does not significantly differ from the refined position (see Table IIIb for the silver mode positions). We are now in position to discuss the silver environments and distances.

The Ag1*–Te distances (see Table V) are homogeneous (from 288 pm to 291 pm) with a mean value $\langle d_{Ag1^*-Te} \rangle = 290$ pm slightly below the ionic radius sum $(r_{Ag^+} + r_{Te^{2-}}) = 299$ pm (*18*), the apparent small squeezing

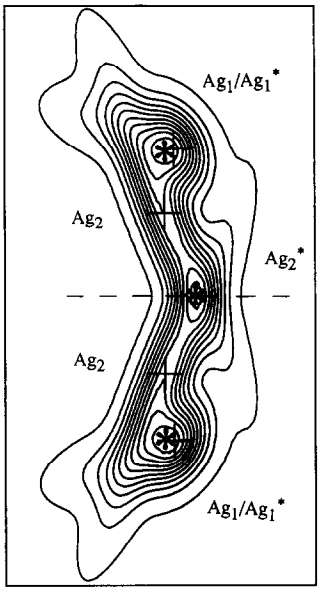

FIG. 3a. Joint probability density function (jpdf) of silver along the direct jump path between two face sharing type IV tetrahedra. The crosses denote the refined atom positions (means) and the stars represent the local maxima (modes). The dashed line indicate the intersection between the plane under view and the triangular common face. Contour lines from 50×10^{-6} pm^{-3} to 2050×10^{-6} in intervals of 200×10^{-6} pm^{-3}.

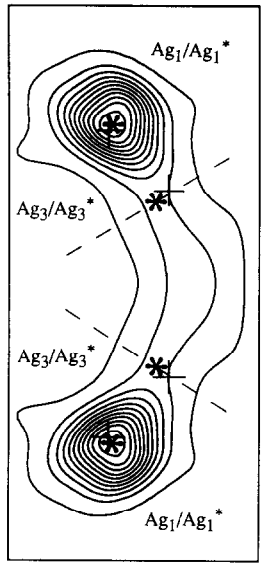

FIG. 3b. Joint probability density function (jpdf) of silver along the indirect jump path between two edge sharing type IV tetrahedra through a type I tetrahedron. The crosses denote the refined atom positions (means) and the stars represent the local maxima (modes). No clear-cut local maxima are observed for the Ag3 atoms. The dashed lines indicate the intersections between the plane under view and the triangular faces common to the type IV and to the type I tetrahedra. Contour lines from 50×10^{-6} pm^{-3} to 2050×10^{-6} pm^{-3} in intervals of 200×10^{-6} pm^{-3}.

resulting from the partial occupancy of the site. Conversely, the Te–Ag1*–Te angles range between 89.3° and 119.4 with a mean value of 108.8°, indicating a strongly distorted tetrahedron.

As could be expected, because of the triangular arrangements of Ag2* and Ag3*, the Ag2*–Te and Ag3*–Te distances are shorter than that observed for Ag1*, e.g., from 239 to 281 pm ($\langle d_{Ag2^*-Te} \rangle$ = 267 pm) and from 256 to 307 pm ($\langle d_{Ag3^*-Te} \rangle$ = 281 pm) for Ag2*–Te and Ag3*–Te, respectively. According to the Ag–Te distance reported by Shannon (*18*) for a silver cation in linear environment, d_{Ag-Te} = 278 pm, one can once again infer from the observed Ag–Te distance shortening an apparent squeezing of the site due to the partial occupancy.

This diffusion path revealed by our refinement solution seems to be the only possible one. This localizes the silver migration within "clusters" built upon 12 type IV tetrahedral sites (see Fig. 4). Four such clusters are observed in each cell (implied by the F centering) and no communication between those clusters seems to be possible. Nevertheless, because of the ionic conductivity character of the phase (similar to that observed by Geller for Ag_8GeTe_6), the cation must be able to move around in the whole structure skeleton. Therefore, in presence of an electric field or at higher temperature there should be a silver migration between the various clusters. Given our current understanding of the structure, it is

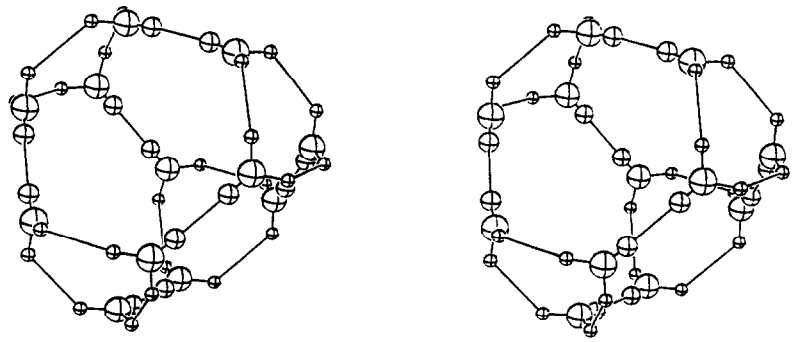

FIG. 4. Ortep stereoscopic view of the silver clusters of γ-Ag_8SiTe_6. Spheres of arbitrary size (large for Ag1, medium for Ag2, and small for Ag3) are used to depict the silver positions (means). Plain lines symbolize direct and indirect diffusion paths.

quite difficult to suggest a given diffusion path between the clusters but we can tentatively consider the type I tetrahedra to constitute such a path. Indeed, two neighboring clusters have in common a type I tetrahedron face, but the present structure determination did not reveal, in the data collection conditions, a residual density in that face.

Let us now demonstrate why some tetrahedral sites can be occupied and why some cannot. Type II tetrahedra cannot be filled because their centers are much too close to silicon position (187 pm). The same argument applies to type I tetrahedra (306 pm from its center to the neighboring silicon atom), but it can be used as a transit site if the migration path stays away from its center. This evidence does not pertain to the other two situations, the centers of the type III and the type V tetrahedra being at 499 pm and 471 pm of the silicon cations, respectively. Those tetrahedra could be filled by silver atoms but then the silver atoms would be trapped in the voids and well localized because the tetrahedra are by far too rigid to allow a jump out of site. Assuredly, to be free to move from one site to another the silver cations need to push away the tellurium anions as they cross the tetrahedral faces and this should show up in the tellurium ADP. As already mentioned, only Te2 and Te3 have high ADP values ($B_{eq} = 5.56 \times 10^4$ pm^2 and $B_{eq} = 4.83 \times 10^4$ pm^2, respectively, compared to $B_{eq} = 1.72 \times 10^4$ pm^2 for Te1 which is linked to Si); therefore, a tetrahedron build upon four Te1, such as a type III tetrahedron, is very inflexible and one made of three Te1 and one Te2, such as a type V tetrahedron, is rather rigid. On the opposite, a tetrahedron with only two Te1 (case of type I and type IV) is more favourable to admit mobile Ag ions. If type III and type V tetrahedra would enclose silver cations (even with a partial small occupancy), those cations should be well localized and thus should show up in a Fourier difference map. This is not the case and we do conclude that those sites are empty.

When we examine the clusters of 12 Ag1* sites (*vide supra*), we calculate a filling of eight silver atoms per cluster. The distance between each silver tetrahedral site is rather small (between 234 and 246 pm) compared to the van der Waals distance between two Ag^+ cations (340 pm) (*26*), but it is not reasonable to consider those distances as true distances in such a disordered structure. A lowering of the temperature should freeze the diffusion movement and should localize the silver atoms among the 42 positions (12 Ag1* sites, 6 Ag2* sites, and 24 Ag3* sites) in an ordered way as found in Ag_8SiS_6 (*16*) and β'-Ag_8GeSe_6 (*27*), that is, with rational Ag–Ag distances (short distances corresponding to d^{10}–d^{10} bonding interactions are not excluded (*12, 16, 27*). The filling of empty sites (type III and V) is also possible. To answer those questions, a study of the powder patterns of the α and β low-temperature phases has been carried on (*vide infra*) and a full structural determination is in progress.

Powder Pattern Analysis of α- and β-Ag_8SiTe_6 Low-Temperature Phases

Experimental. A low-temperature DSC measurements confirmed the results of Gorochov (*8*), e.g., the successive allotropic, reversible phase transformations:

(1) α-$Ag_8SiTe_6 \xrightarrow{195\ K} \beta$-$Ag_8SiTe_6$

(2) β-$Ag_8SiTe_6 \xrightarrow{263\ K} \gamma$-$Ag_8SiTe_6$ (stable from room temperature to its melting point).

Our measurements clearly show two well-defined first-order transition peaks.

The powder samples for the low-temperature X-ray studies have been prepared as described for the γ phase but without inter-

nal standards. The measurements were undertaken on the same diffractometer outfitted with a low temperature Anton–Paar chamber, operating with a liquid nitrogen flow. The data were scanned in steps of 0.03° (2θ) with 50-sec counting periods over a 5°–89° range (2θ). Three measurements were performed: one at room temperature for the γ phase, one at 213 K for the β phase, and the last one at 163 K for the α phase.

Analysis and discussion. As already observed by Gorochov (*8*), the low-temperature powder patterns show small peaks which attest the phase transitions and which cannot be indexed with the γ phase cubic lattice cell parameter a. In 1981, Katty *et al.* (*28*) suggested for the β-Ag_8GeTe_6 phase a primitive quadratic cell with the following parameters $a' = b' \approx 4a$ and $c' \approx 2a$, e.g. 32 times the "F centered cubic" (*vide supra*) cell of γ-Ag_8GeTe_6.

With the Prolix and Disindaf programs (*13*) (on a peak-by-peak basis) we could index all the lines of the α and β phase powder patterns in a cubic primitive cell with the parameter $a' \approx 2a$. Given the complexity of the powder patterns (strong peak overlap in high 2θ region), we preferred a full pattern matching procedure (*29*). Thus, the three powder patterns were refitted with the Fullprof program (*30*). The final refinements without structural information included the cell constants, the zero-point, two halfwidth parameters ($FWHM^2 = V^*\tan(\theta) + W$), the two mixing parameters of the pseudo-Voigt peak-shape function ($\eta = \eta_0 + \chi^*2\theta$); the background was linearly interpolated between 52 points. The results (e.g., Laue class, cell parameters, number of reflections, and refinement criteria) are gathered in Table VI. In Table VII can be found the *hkl* lists for the three phases in the 5°–60° 2θ range. In this chosen angular range, we note 16 and 61 additional lines for the β and α phases as compared to the γ phase diagram.

A small discrepancy is observed between the cell parameter of the γ phase obtained on the one hand with the Prolix/Disindaf programs (a = 1152.25(7) pm, with an internal standard correction) and on the other hand with the Fullprof program (1151.75(7) pm, without internal standard correction). Nevertheless, the set of parameters we calculated from the three-phase powder patterns is homogeneous, in the sense that we observe a shrinking of the parameter as a

TABLE VI

RESULTS OF THE REFINEMENTS WITH THE FULLPROF PROGRAM

	γ-phase	β-phase	α-phase
Laue Class	*Fm3m*	*Pm3m*	*Pm3m*
a (pm)	1151.75(7)	2301.7(1)	2298.4(1)
R_p	11.5	11.5	11.3
R_{wp}	14.6	14.6	14.7
χ^2	2.48	2.21	1.69
R_{exp}	9.24	9.84	11.3
N − P + C	946	1399	2063
With: The Profile		$R_p = 100\,\Sigma_i\lvert y_i - y_{ci}\rvert/\Sigma_i\lvert y_i\rvert$	
The weighted profile		$R_{wp} = 100[\Sigma_i w\lvert y_i - y_{ci}\rvert^2/\Sigma_i w y_i^2]^{1/2}$	
The expected		$R_{exp} = 100[(N - P + C)/\Sigma_i w y_i^2]^{1/2}$	
The goodness of fit		$\chi^2 = [R_{wp}/R_{exp}]^2$	
The number of degrees of freedom: N − P + C with		N: the number of points in the pattern P: the number of refined parameters C: the number of constraint functions.	

TABLE VII

INDEXED POWDER PATTERNS OF THE α-, β-, AND γ-Ag_8SiTe_6 PHASES IN THE 0–60° 2θ RANGE

γ phase			β phase			α phase		
$h\ k\ l$	$2\theta_{cal}$	I_{rel}	$h\ k\ l$	$2\theta_{cal}$	I_{rel}	$h\ k\ l$	$2\theta_{cal}$	I_{rel}
						2 1 1	9.42	<1
						3 1 0	12.17	<1
1 1 1	13.30	5	2 2 2	13.31	5	2 2 2	13.33	6
			3 2 0	13.86	<1	3 2 0	13.88	1
						3 2 1	14.41	<1
2 0 0	15.37	<1	4 0 0	15.38	<1	4 0 0	15.41	<1
						3 3 0 4 1 1	16.35	<1
						3 3 1	16.80	<1
						4 2 1	17.67	<1
						3 3 2	18.09	<1
						5 1 0 4 3 1	19.68	<1
						5 1 1 3 3 3	20.06	<1
			5 2 0 4 3 2	20.76	<1	5 2 0 4 3 2	20.79	3
2 2 0	21.81	<1	4 4 0	21.82	<1	4 4 0	21.86	<1
						5 3 1	22.87	<1
3 1 1	25.63	35	6 2 2	25.65	34	6 2 2	25.69	34
			6 3 0 5 4 2	25.94	<1	6 3 0 5 4 2	25.98	3
2 2 2	26.79	100	4 4 4	26.81	100	4 4 4	26.85	100
			7 2 0 6 4 1	28.20	<1	7 2 0 6 4 1	28.24	5
			7 2 1 5 5 2 6 3 3	28.47	<1	7 2 1 5 5 2 6 3 3	28.51	<1
						6 4 2	29.05	<1
						7 3 0	29.57	<1
						7 3 1 5 5 3	29.83	1
						6 5 0 6 4 3	30.35	1
						6 5 1 7 3 2	30.60	2
						8 1 1 7 4 1 5 5 4	31.60	3
						7 3 3	31.84	<1
						8 2 0 6 4 4	32.09	<1
			8 2 1 7 4 2	32.28	1	8 2 1 7 4 2	32.33	10
						6 5 3	32.57	<1
						7 5 0 8 3 1 7 4 3	33.51	1
			7 5 1 5 5 5	33.69	1	7 5 1 5 5 5	33.74	4

TABLE VII—*Continued*

γ phase			β phase			α phase		
h k l	$2\theta_{cal}$	I_{rel}	*h k l*	$2\theta_{cal}$	I_{rel}	*h k l*	$2\theta_{cal}$	I_{rel}
3 3 1	33.90	8	6 6 2	33.92	9	6 6 2	33.98	8
			8 3 2 6 5 4	34.15	2	8 3 2 6 5 4	34.21	15
			7 5 2	34.38	<1	7 5 2	34.43	<1
4 2 0	34.81	4	8 4 0	34.83	3	8 4 0	34.89	4
						9 1 1 7 5 3	35.56	1
						9 2 1 7 6 1 6 5 5	36.21	1
						8 5 0 9 2 2 7 6 2 8 4 3	36.86	<1
						9 3 0 8 5 1 7 5 4	37.08	2
						9 3 1	37.29	<1
						8 5 2	37.71	1
			9 3 2 7 6 3	37.86	<1	9 3 2 7 6 3	37.92	2
4 2 2	38.25	27	8 4 4	38.28	24	8 4 4	38.34	18
						9 4 0 6 6 5	38.55	1
			7 7 1 9 3 3 7 5 5	38.90	<1	7 7 1 9 3 3 7 5 5	38.96	1
			10 1 0 8 6 1 9 4 2 7 6 4	39.31	3	10 1 0 8 6 1 9 4 2 7 6 4	39.37	13
						10 1 1 7 7 2	39.57	2
						9 5 0 9 4 3	40.37	2
			9 5 1 7 7 3	40.50	5	9 5 1 7 7 3	40.57	3
5 1 1 3 3 3	40.67	99	10 2 2 6 6 6	40.70	71	10 2 2 6 6 6	40.77	85
			10 3 0 8 6 3	40.90	4	10 3 0 8 6 3	40.96	4
						10 3 1 9 5 2 7 6 5	41.16	3
						9 5 3	42.13	1
						9 6 0 10 4 1 8 7 2	42.51	<1
						11 1 0 8 7 3 9 5 4	43.45	<1
						11 1 1 7 7 5	43.64	<1

TABLE VII—*Continued*

γ phase			β phase			α phase		
h k l	$2\theta_{cal}$	I_{rel}	*h k l*	$2\theta_{cal}$	I_{rel}	*h k l*	$2\theta_{cal}$	I_{rel}
						11 2 0 10 5 0 10 4 3 8 6 5	44.01	<1
						11 2 1 10 5 1 9 6 3	44.20	<1
4 4 0	44.46	47	8 8 0	44.49	30	8 8 0	44.56	33
						8 8 1 11 2 2 10 5 2 8 7 4	44.75	<1
						9 6 4	45.47	1
5 3 1	46.62	11	10 6 2	46.65	8	10 6 2	46.72	10
						11 4 2 10 5 4	46.90	<1
4 4 2 6 0 0	47.32	5	8 8 4 12 0 0	47.35	4	8 8 4 12 0 0	47.43	4
						11 5 1 7 7 7	47.95	<1
						10 7 0 12 2 1 9 8 2 8 7 6	48.30	3
6 2 0	50.05	5	12 4 0	50.08	3	12 4 0	50.16	4
5 3 3	52.02	8	10 6 6	52.06	6	10 6 6	52.15	10
						13 2 0 12 5 2 10 8 3 11 6 4	52.31	2
6 2 2	52.67	11	12 4 4	52.71	8	12 4 4	52.80	11
4 4 4	55.21	<1	8 8 8	55.25	<1	8 8 8	55.34	4
						14 1 0 12 7 2 10 9 4	56.12	1
			11 9 1 13 5 3	56.95	<1	11 9 1 13 5 3	57.04	<1
7 1 1 5 5 1	57.06	3	14 2 2 10 10 2	57.10	2	14 2 2 10 10 2	57.20	3
			14 3 0 13 6 0 12 6 5	57.26	<1	14 3 0 13 6 0 12 6 5	57.35	<1
						14 5 0 11 10 0 14 4 3 13 6 4 11 8 6	59.76	2
						14 5 1 11 10 1 13 7 2	59.91	<1

function of the lowering of temperature ($2a$ = 2303.4 pm → a = 2301.7 pm → a = 2298.4 pm).

Concluding Remarks

In this structure determination, although we clearly located the main silver sites and we foresaw what could be the main silver diffusion paths in clusters, we could not unravel the overall difusion process, that is, the diffusion between these silver clusters. One possible reason could be linked to the relative low ionic conductivity at the temperature of the single crystal X-ray study (room temperature), that is, a few degrees above the γ to β transition. To completely determine the diffusion silver process in γ-Ag_8SiTe_6, and in the γ-Ag_8MX_6 phases in general, a complete study of the anharmonic vibration of silver cations as well as ionic conductivity measurements as a function of temperature is under way.

References

1. R. J. Cava, F. Reidinger, and B. J. Wuensch, *Solid State Commun.* **24,** 411 (1977).
2. T. Sakuma and S. Saitoh, *J. Phys. Soc. Jpn.* **54,** 3647 (1985).
3. R. Rahlfs, *Z. Phys. Chem. B* **31,** 157 (1936).
4. H. Hahn, H. Schulze, and L. Sechser, *Naturwissenschaften* **52,** 451 (1965).
5. O. Gorochov, R. Fichet, and J. Flahaut, *C.R. Acad. Sci. Paris, Ser. C* **263,** 1422 (1966).
6. O. Gorochov and J. Flahaut, *C.R. Acad. Sci. Paris, Ser. C* **264,** 2153 (1967).
7. O. Gorochov, *C.R. Acad. Sci. Paris, Ser. C* **266,** 1059 (1968).
8. O. Gorochov, *Bull. Soc. Chim. Fr.* **6,** 2263 (1968).
9. N. Rysanek, P. Laruelle, and A. Katty, *Acta. Crystallogr., Sect. B* **32,** 692 (1976).
10. J. von Unterrichter and K. J. Range, *Z. Naturforsch., B: Anorg. Chem., Org. Chem.* **33,** 866 (1978).
11. S. Geller, *Z. Kristallogr.* **149,** 31 (1979).
12. M. Jansen, *Angew. Chem. Int. Ed. Engl.* **26,** 1098 (1987).
13. P. Deniard, M. Evain, J. M. Barbet, and R. Brec, "Transtec Publication Materials Science," conference report, in press.
14. C. Kay Fair, "MOLEN: Structure Determination Package," Enraf-Nonius (1982).
15. G. Ouvrard, E. Sandre, and R. Brec, *J. Solid State Chem.*, **73,** 27 (1988).
16. B. Krebs and J. Mandt, *Z. Naturforsch., B: Anorg. Chem., Org. Chem.* **32,** 373 (1977).
17. H. Vincent, D. Leroux, D. Bijaoui, R. Rimet, and C. Schlenker, *J. Solid State Chem.* **63,** 349 (1986).
18. R. D. Shannon, "Structure and Bonding in Crystals" (M. O'Keeffe and A. Navrotsky, Eds.), Vol. 2, p. 61, Academic Press, San Diego (1981).
19. M. Barj, G. Lucazeau, G. Ouvrard, and R. Brec, *Eur. J. Solid State Inorg. Chem.* **25,** 449 (1988).
20. S. Lee, P. Colombet, G. Ouvrard, and R. Brec, *Mater. Res. Bull.* **21,** 917 (1986).
21. P. Toffoli, P. Khodadad, and N. Rodier, *Acta Crystallogr. Sect. C* **39,** 1485 (1983).
22. E. Prouzet, G. Ouvrard, and R. Brec, *Mater. Res. Bull.* **21,** 195 (1986).
23. R. Bachmann and H. Schulz, *Acta. Crystallogr. Sect. A* **40,** 668 (1984).
24. U. H. Zucker, E. Perenthaler, W. F. Kuhs, R. Bachmann, and H. Schulz, *J. Appl. Crystallogr.* **16,** 358 (1983).
25. W. F. Kush, *Acta Crystallogr., Sect. A* **39,** 148 (1983).
26. A. Bondi, *J. Phys. Chem.* **68,** 441 (1964).
27. D. Carré, R. Ollitrault-Fichet, and J. Flahaut, *Acta Crystallogr., Sect. B* **36,** 245 (1980).
28. A. Katty, O. Gorochov, and J. M. Letoffe, *J. Solid State Chem.* **38,** 259 (1981).
29. G. S. Powley, *J. Appl. Crystallogr.* **14,** 357 (1981).
30. J. Rodriguez-Carvajal, "FULLPROF: A Program for Profile Refinement of constant Wavelength X-ray and Neutron Powder Diffraction Patterns," ILL Grenoble, France (1991).